

# Stable bright solitons in two-component Bose-Einstein condensates

A.I. Yakimenko<sup>1,2</sup>, K.O. Shchebetovska<sup>1</sup>, S.I. Vilchinskii<sup>1</sup>, M. Weyrauch<sup>3</sup>

<sup>1</sup> *Department of Physics, Taras Shevchenko National University, Kiev 03022, Ukraine*

<sup>2</sup> *Institute for Nuclear Research, Kiev 03680, Ukraine*

<sup>3</sup> *Physikalisch-Technische Bundesanstalt, Bundesallee 100, D-38116 Braunschweig, Germany*

Two-dimensional (2D) fundamental soliton-soliton pairs are investigated in two-component Bose-Einstein condensates with attractive interactions between the atoms of the same sort. Both attractive and repulsive interactions between atoms of the different components are considered. The general properties of the stationary states are investigated analytically and numerically. The region of stability of the soliton-soliton pairs are found.

PACS numbers: 05.45.Yv, 03.75.Lm, 05.30.Jp

## I. INTRODUCTION

Multicomponent Bose-Einstein condensates (BECs) have been subject of growing interest in recent years as they open intriguing possibilities for a number of important physical applications, including coherent storage and processing of optical fields, quantum simulation, quantum interferometry *etc.* Experimentally, multicomponent BECs can be realized by simultaneous trapping of different species of atoms or atoms of the same isotope in different hyperfine states. Theoretical models of multicomponent BECs in the mean-field approximation are formulated in the framework of coupled Gross-Pitaevskii (GP) equations and the order parameter of multicomponent BECs is described by a multicomponent vector.

Like in the scalar condensate case, various types of nonlinear matter waves have been predicted in multicomponent BECs. Two-dimensional (2D) and three-dimensional (3D) vector solitons and vortices have been considered previously for the case of repulsive condensates. Recent investigations [3] theoretically predict existence of stable soliton-vortex pairs for the case of attractive intracomponent interaction. However, the ground state of two-component 2D BECs with external trapping potential remain not investigated yet. Note, that the soliton-soliton pairs have been very recently investigated in the frame of two coupled NLSE with self-focusing and cross-defocusing interactions and with no linear potential [4]. It was found in Ref. [4] that the bright vector solitons are unstable and more powerful component collapse in the end. It is reasonable to expect that a final stabilization could be obtained with additional trapping potential.

In this work we perform a detailed theoretical analysis of soliton-soliton matter-wave nonlinear structures for attractive intracomponent interactions and different signs of intercomponent interactions. General properties of the steady states are investigated analytically by means of variational analysis and compared with numerical simulations. The existence and stability domains of soliton-soliton matter-wave vector solitons are found.

## II. BASIC EQUATIONS

We consider a binary mixture of two BECs which is described at the limit  $T \rightarrow 0$  in mean-field approximation by set of GP equations:

$$i\hbar \frac{\partial \Psi_1}{\partial t} = \left[ \hat{H}_1 + g_{11} |\Psi_1|^2 + g_{12} |\Psi_2|^2 \right] \Psi_1, \quad (1)$$

$$i\hbar \frac{\partial \Psi_2}{\partial t} = \left[ \hat{H}_2 + g_{21} |\Psi_1|^2 + g_{22} |\Psi_2|^2 \right] \Psi_2, \quad (2)$$

where  $\hat{H}_j = -\frac{\hbar^2}{2M_j} \nabla^2 + V_j(\mathbf{r})$ ,  $M_j$  is the mass of the atoms in  $j$ -th component,  $V_j(\mathbf{r}) = M_j \omega_{\perp}^2 (x^2 + y^2)/2 + M_j \omega_z^2 z^2/2$  is the axially-symmetric harmonic external trapping potential. Atom-atom interactions of the same sort are characterized by the coupling coefficients  $g_{jj} = 4\pi \hbar^2 a_{jj}/M_j$ , where  $a_{jj}$  are the  $s$ -wave scattering lengths for binary collisions between atoms. The coupling coefficient of intercomponent interaction is  $g_{12} = g_{21} = 2\pi \hbar^2 a_{12}/M_*$ , where  $M_* = M_1 M_2 / (M_1 + M_2)$  is the reduced mass.

We assume that  $\omega_z \gg \omega_{\perp}$  and the nonlinear interactions are weak relative to the confinement in the longitudinal (along  $z$ -axis) direction. In this case, the BEC is a "disk-shaped" one. The longitudinal motions of condensates are assumed to be frozen:  $\Psi_j(\mathbf{r}, t) = \tilde{\Psi}_j(x, y, t) \Upsilon_j(z, t)$ , where  $\Upsilon_j(z, t) = (l_{zj} \sqrt{\pi})^{-1/2} \exp(-\frac{i}{2} \omega_z t - \frac{1}{2} z^2 / l_{zj}^2)$  is the ground state wave function of the longitudinal harmonic trapping potential,  $l_{zj} = \sqrt{\hbar / (M_j \omega_z)}$ . After integrating out the longitudinal coordinates the GP equations take an effectively 2D form:

$$i \frac{\partial \tilde{\Psi}_j}{\partial t} + \left( \hat{h}_j + |\tilde{\Psi}_j|^2 + b_{j,3-j} |\tilde{\Psi}_{3-j}|^2 \right) \tilde{\Psi}_j = 0, \quad (3)$$

where  $j = 1, 2$ ,  $\hat{h}_1 = \Delta_{\perp} - r^2$ ,  $\hat{h}_2 = \kappa \Delta_{\perp} - \frac{r^2}{\kappa}$ ,  $\kappa = M_1 / M_2$ ,  $r = \sqrt{x^2 + y^2}$ ,  $\Delta_{\perp} = \partial^2 / \partial x^2 + \partial^2 / \partial y^2$  is the 2D Laplacian. Here we have introduced the dimensionless variables:  $(x, y) \rightarrow (x, y) / l_{\perp 1}$ ,  $t \rightarrow t / \tau$ ,  $\tilde{\Psi}_j \rightarrow \tilde{\Psi}_j / \sqrt{C_j}$ , where  $l_{\perp 1} = \sqrt{\hbar / (M_1 \omega_{\perp})}$ ,  $\tau = 2 / \omega_{\perp}$ ,

$C_j = \hbar\omega_\perp \sqrt{\pi(l_{z1}^2 + l_{z2}^2)} / (2|g_{jj}|)$ . Dimensionless coupling parameters are defined as follows:  $b_{12} = -\frac{g_{12}}{|g_{11}|} \sqrt{\frac{2}{1+\kappa}}$ ,  $b_{21} = -\frac{g_{21}}{|g_{22}|} \sqrt{\frac{2\kappa}{1+\kappa}}$ . For simplicity we consider here the symmetric case  $M_1 = M_2$  and  $g_{11} = g_{22}$ , so that  $\kappa = 1$ ,  $b_{12} = b_{21} = \sigma$ . Here we are interested in cases where the diagonal part of the interaction matrix  $g_{ij}$  is attractive ( $g_{11} < 0$ ,  $g_{22} < 0$ ) while the off-diagonal terms  $g_{12} = g_{21}$  may be attractive ( $g_{12} < 0$ ) or repulsive ( $g_{12} > 0$ ).

Equations (1) and (2) have the integrals of motion:

(i) number of particles in each component

$$N_j = \int |\tilde{\Psi}_j|^2 d^2\mathbf{r}, \quad (4)$$

(ii) energy functional

$$E = E_1 + E_2 - \sigma \int |\tilde{\Psi}_1|^2 |\tilde{\Psi}_2|^2 d^2\mathbf{r}, \quad (5)$$

where

$$E_j = \int \left\{ |\nabla \tilde{\Psi}_j|^2 + r^2 |\tilde{\Psi}_j|^2 - \frac{1}{2} |\tilde{\Psi}_j|^4 \right\} d^2\mathbf{r},$$

(iii) momentum, and (iv) angular momentum.

Stationary soliton solutions are given as follows:

$$\tilde{\Psi}_j(\mathbf{r}, t) = \psi_j(r) e^{-i\mu_j t}, \quad (6)$$

where  $r = \sqrt{x^2 + y^2}$ ,  $\mu_j$  are chemical potentials, and real functions  $\psi_j(r)$  satisfy the set of equations:

$$\mu_j \psi_j + \psi_j'' + \frac{1}{r} \psi_j' - r^2 \psi_j + [\psi_j^2 + \sigma \psi_{3-j}^2] \psi_j = 0. \quad (7)$$

At fixed strength of inter-component interaction  $\sigma$  we obtain two-parameter family (with parameters  $\mu_1$  and  $\mu_2$ ) of vector soliton solutions.

In the next sections we consider stationary states and investigate their stability for attractive ( $\sigma > 0$ ) and for repulsive ( $\sigma < 0$ ) interparticle interactions.

### III. STATIONARY SOLUTIONS

#### A. Attractive intercomponent interactions ( $\sigma > 0$ )

Equations (7) were solved by the stabilized relaxation method similar to that described in Ref. [7]. To gain a better insight into the properties of the vector solitons we have performed also the variational analysis of the stationary vector fundamental solitons. The variational results provide not only an appropriate initial guesses for our numerical relaxation procedure but also they exhibit a good agreement with numerical calculations, as is seen from Figs. 1 and 2.

Since for attractive interparticle interactions both solitonic components are basically bell-shaped, a simple trial function of the form:

$$\psi_j(r) = \sqrt{\frac{N_j}{\pi a_j^2}} e^{-\frac{1}{2} \frac{r^2}{a_j^2}}, \quad (8)$$

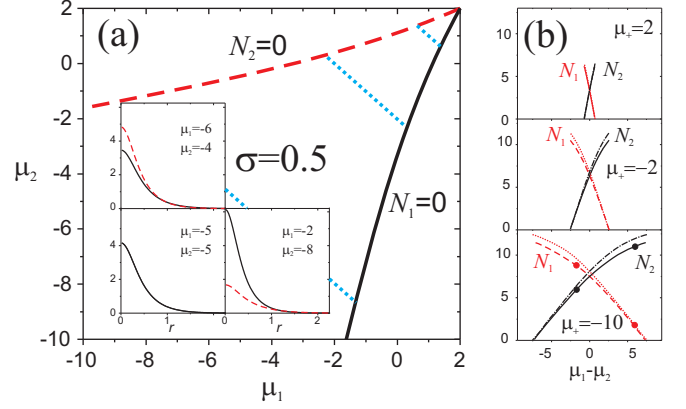


FIG. 1: (Color online) Stationary fundamental vector solitons with weak attractive intercomponent interactions ( $\sigma = 0.5$ ) (a) Existence region on the plane of chemical potentials ( $\mu_1, \mu_2$ ). (b) The number of atoms  $N_1$  (red dashed line for numerical results and dotted red line for variational results) and  $N_2$  (solid black line for numerical results dash-dotted black line for variational results). The number of atoms are presented as the functions of difference between chemical potentials  $\mu_- = \mu_1 - \mu_2$  at different values of total chemical potential  $\mu_+ = \mu_1 + \mu_2$ . The insets give the examples of radial profiles  $\psi_1(r)$  (dashed red line) and  $\psi_2(r)$  (solid black line) for the points indicated on the last diagram  $N_1(\mu_-)$  and  $N_2(\mu_-)$ .

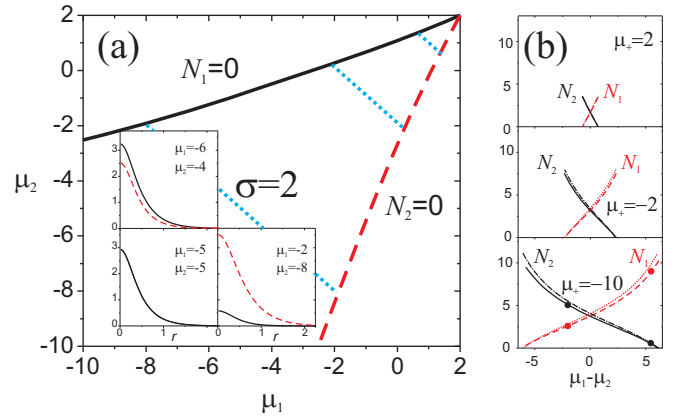


FIG. 2: (Color online) The same as in Fig. 1 for  $\sigma = 2.0$ .

is expected to be a good approximation. Here  $a_j$  is the effective width of  $j$ -th component. The trial function is normalized on the number of particles:  $\langle \psi_j | \psi_j \rangle = N_j$ . Substituting the trial function (8) into Eq. (5), we get for the energy functional  $E$

$$E = E_1 + E_2 - \sigma E_{12}, \quad (9)$$

where

$$E_j = N_j \left( \frac{1}{a_j^2} + a_j^2 - \frac{N_j}{4\pi a_j^2} \right), \quad E_{12} = \frac{N_1 N_2}{\pi(a_1^2 + a_2^2)}.$$

A soliton solution corresponds to the stationary point of the energy functional at fixed number of particles in both components:  $(\partial E / \partial a_1)_{N_1, N_2} = 0$ ,  $(\partial E / \partial a_2)_{N_1, N_2} = 0$ .

Obviously, a two-parameter family of the vector soliton are symmetric with respect to simultaneous replacement  $\mu_1 \rightarrow \mu_2$  and  $\psi_1 \rightarrow \psi_2$ , so in the plane of chemical potentials  $(\mu_1, \mu_2)$  the solutions are symmetric with respect to the line  $\mu_1 = \mu_2$ . To utilize this symmetry we present the number of particles for each component as the functions of difference between chemical potentials  $\mu_- = \mu_1 - \mu_2$  at fixed total chemical potential  $\mu_+ = \mu_1 + \mu_2$ . The typical diagrams are given in Fig. 1 (b) and Fig. 2 (b). Note that the existence region of the vector soliton-soliton pairs is restricted, and beyond this region only single-component (scalar) solitons exist. The diagrams from Fig. 1 (b) and Fig. 2 (b) correspond to the cuts  $\mu_+ = \text{const}$  indicated by dotted blue lines in Fig. 1 (a) and Fig. 2 (a). For different fixed values of  $\mu_+$  we have found the corresponding diagrams and finally reconstructed all the existence region. When the strength of interaction  $\sigma$  increases, the region of existence shrinks gradually while at  $\sigma = 1$  the lines merge. Indeed, only scalar solitons exist in the case  $\sigma = 1$ . When the parameter  $\sigma$  increases above one (intercomponent interactions are going to dominate over intracomponent interactions in this case), then the existence region of vector solitons grows. Note the lines, which restrict this region for  $\sigma > 1$ , swap around in comparison with the case  $0 < \sigma < 1$  [compare Fig. 1 (a) and Fig. 2 (a)].

In the point  $\mu_1 = \mu_2 = 2$  both solitonic components vanish as it must be since the linear effects dominate here. It is also to easy to show that the solutions with the same number of atoms with  $\mu_- = 0$  is the of the same structure as it is for single-component GPE with the effective strength of interaction  $\tilde{\sigma} = 1 + \sigma$ , so the number of atoms at the line  $\mu_- = 0$  will grow from zero at point  $\mu_1 = \mu_2 = 2$  and saturate at the value  $N_{max} = N_{cr}/(1 + \sigma)$  if  $\mu_1 = \mu_2 \rightarrow -\infty$ .

As is seen from Fig. 1 (b) and Fig. 2 (b), the maximum number of particles  $N_{j\ max}$  in one component grows with distance from the point  $\mu_1 = \mu_2 = 2$ , and number of atoms reaches its peak value ( $N_j \rightarrow N_{j\ max}$ ) at the edge of the existence domain where another component degenerates ( $N_{3-j} \rightarrow 0$ ). It is remarkable that when nonlinear effects dominate, the behavior of dependencies  $N_j(\mu_-)$  are qualitatively different for the weak and strong interparticle interactions. In the first case ( $0 < \sigma < 1$ ) number of atoms saturates at the maximum value of single-component soliton  $N_{j\ max} \leq N_{cr}$ . Here  $N_{cr}$  is the critical number of particles of untrapped BEC with attractive interparticle interactions. As known,  $N_{cr} = 11.68$  or in variational approach with the trial function of the form (8) BEC  $N_{cr} = 4\pi$ . In the case ( $\sigma > 1$ ) the number of atoms decay dramatically from the value  $N_{j\ max} \leq N_{cr}$  at the one edge to zero at the other edge of the existence domain. As the result, the total number of particles in both components for the case of dominating intercomponent interactions ( $\sigma > 1$ ) is less than critical value:  $N = N_1 + N_2 < N_{cr}$ . If the inter-component interactions are weak ( $0 < \sigma < 1$ ), the total number of particles in vector soliton-soliton pair can be greater than  $N_{cr}$ . The

similar effect has been noted for optical vector solitons in media with focusing nonlinearities [6].

## B. Repulsive intercomponent interactions ( $\sigma < 0$ )

A variational procedure with simple gaussian ansatz gives a good analytical approximation for stationary solutions for attractive interparticle interactions. However, it fails to describe a state of vector solitons with spatially separated components, which appear for repulsive intercomponent interactions. A simplest normalized trial function that include a possibility for modification of a soliton shape is as follows:

$$\psi_j(r) = A_j \left( 1 + \delta_j \frac{r^2}{a_j^2} \right) e^{-\frac{1}{2} \frac{r^2}{a_j^2}}, \quad (10)$$

where  $a_j$  is the effective width of  $j$ -th component of soliton-soliton pair,  $A_j = \sqrt{N_j/(\pi a_j^2(1 + 2\delta_j(1 + \delta_j)))}$ . The parameter  $\delta_j \geq 0$  introduces alterations of soliton shape from a gaussian-type profile. If  $\delta_j > 1/2$ , the density distribution has a local minima at the soliton center. Evidently only one BEC component at once can be forced out by repulsive intercomponent interaction, which is why one of the parameters, say  $\delta_2$  is set equal to zero without the loss of generality As the result we have only three variational parameters to be determined:  $a_1, a_2$  and  $\delta = \delta_1$ . Using the described above variational procedure we have obtained approximate stationary solutions.

Remarkable feature of BECs with repulsive intercomponent interaction is multistability of steady-state solutions. In the frame of the variational approach it is easy to show that for the same values of the chemical potentials  $\mu_1$  and  $\mu_2$  the solutions with  $\delta > 0$  can coexist with bell-shaped vector solitons having  $\delta = 0$ . Indeed, as is seen from Fig. 4, solutions with  $\delta = 0$  (solid curves) and with  $\delta > 0$  (dashed curves) become widely separated at the edge of existence domain. Note that for solutions with close values of chemical potential (when  $\mu_- = \mu_1 - \mu_2 \approx 0$ ) these two solitonic branches can be merged as in Fig 4 for  $\mu_+ = 2.0$  and  $\mu_+ = 0.5$ .

When the nonlinear effects are strong (far from the point  $\mu_1 = \mu_2 = 2$ ), the absolute values of the derivatives  $|\partial N_j / \partial \mu_j|$  grows rapidly in the vicinity of the intersection point (see Fig. 4). It is remarkable, that in a curve  $N_j(\mu_-)$  a fold appears, if  $N_j(0) > 16\pi/(3 + \sigma)$  and the coupling constant  $-1 < \sigma < -1/3$ . In this case two additional crossing points are observed at  $\mu_1 = \mu_2$ . The fold in the diagrams  $N_j(\mu_-)$  occurs provided  $\mu_+ < -4(3 + 5\sigma)/\sqrt{(3 + \sigma)(-1 - 3\sigma)}$  for solutions with  $\delta = 0$ : there are *three* stationary solutions in the vicinity of the point  $\mu_- = 0$ . As it must be the diagrams are symmetric with respect to replacement  $\mu_1 \rightarrow \mu_2$  and  $\psi_1 \rightarrow \psi_2$ . The typical examples of the diagram with "multistability" is given in Fig. 4 for  $\mu_+ = -3$ . Note

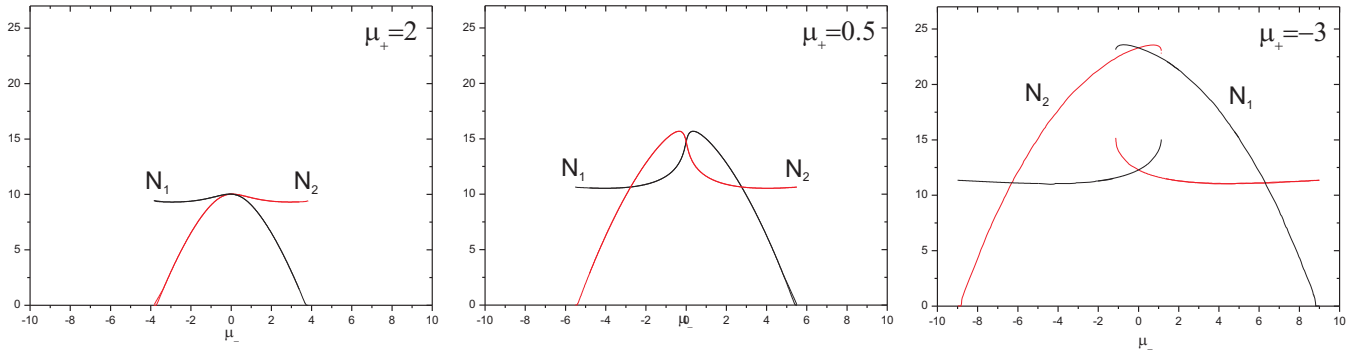


FIG. 3: (Color online) Number of atoms vs  $\mu_- = \mu_1 - \mu_2$  and different  $\mu_+ = \mu_1 + \mu_2$  ( $\sigma = -0.5$ , numerical results).

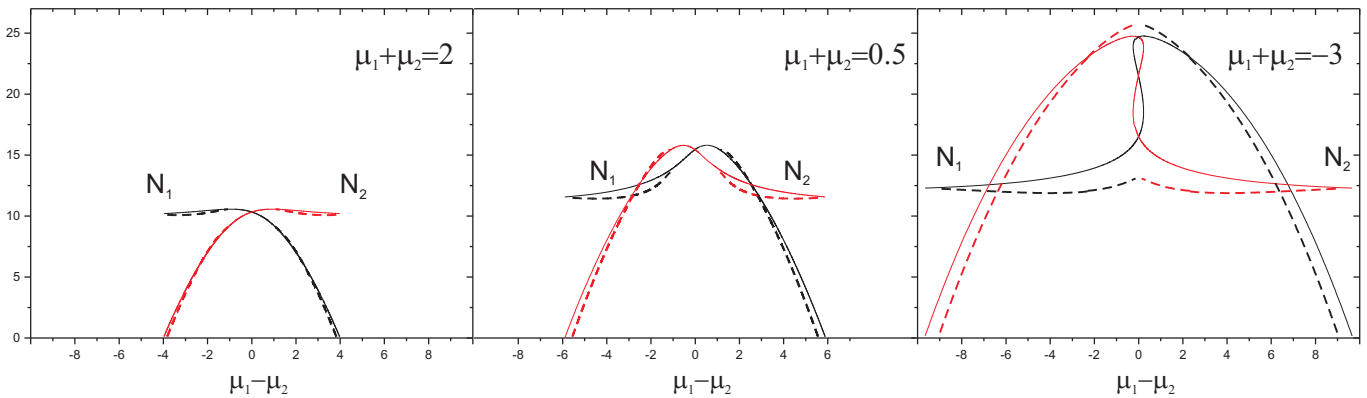


FIG. 4: (Color online) Variational results for  $\sigma = -0.5$ . Number of atoms  $N_1$  (black curves) and  $N_2$  (red curves) vs  $\mu_- = \mu_1 - \mu_2$  and different  $\mu_+ = \mu_1 + \mu_2$ . Solid curves correspond to variational solutions with  $\delta = 0$ , dashed curves indicate solutions with  $\delta > 0$ .

that the folded diagrams occur in unstable region (see below).

#### IV. STABILITY ANALYSIS

We have investigated stability of the obtained stationary solutions by three methods:

(i) Some general conclusions concerning stability follows from variational procedure. Indeed, it is easy to find a sufficient condition for radially-symmetric collapse. From variational results follows that if each solitonic component satisfies the condition  $N_j < N_{cr} = 4\pi$ , then stationary point of the Hamiltonian (which is found from the conditions  $(\partial E / \partial a_j)_{N_1, N_2} = 0$ ,  $(\partial E / \partial \delta)_{N_1, N_2} = 0$ ) corresponds to the Hamiltonian's minimum. However, the saddle point replace the extremum and corresponding steady states are expected to be unstable, if  $N_j > N_{cr}$ .

These observations predicts complete stability with respect to radially-symmetric collapse of the soliton-soliton pairs for attractive intercomponent interactions, since in this case both components always have number of particles below the critical value (see Figs. 1 (b) and 2 (b)). At the same time, for repulsive interparticle interactions

condition  $N_j < N_{cr}$  is fulfilled only in the vicinity of edge of existence domain (see Fig. 5, where blue line is the boundary of the collapse-free region).

(ii) Stability of the stationary solutions with respect to azimuthal symmetry-breaking perturbations was investigated by linear stability analysis. We represent order parameter of two-component BEC in the form  $\tilde{\Psi}_j(r, t) = (\psi_j(r) + \varepsilon_j(r, t))e^{-\mu_j t}$ , where small perturbation  $\varepsilon_j(r, t)$  has the form  $\varepsilon_j(r, t) = u_j(r)e^{i\omega t + iL\varphi} + v_j^*(r)e^{-i\omega^* t - iL\varphi}$ . We linearized equations with respect to  $\varepsilon$  and solved obtained eigenvalue problem for  $\omega$ .

It is found that the growth rates  $\gamma_L = \text{Im}(\omega) = 0$ , that predicts stability of the stationary states if interparticle interaction is attractive.

For repulsive interparticle interactions azimuthal modes  $L = 1$  and  $L = 2$  can be unstable. The example diagram of the maximum growth rates as the function of chemical potential  $\mu_2$  at fixed  $\mu_1$  is given in Fig. 6. Note that above some threshold value of  $\mu_2$  all growth rates vanish. It is remarkable also that mode  $L = 1$  has much more wider instability region and the growth rates of the mode  $L = 2$  are less than the growth rates of the mode  $L = 1$ . That is why modes  $L = 1$  are most dangerous for stability of the solitons with repul-

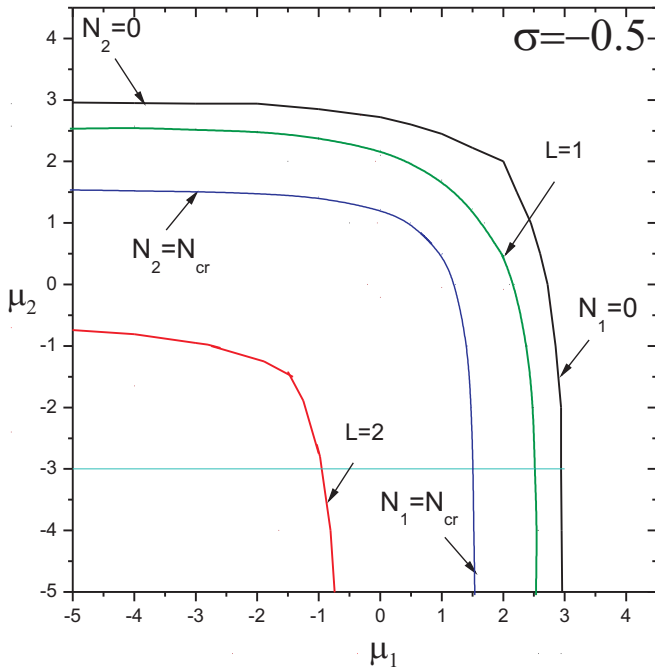


FIG. 5: (Color online) Existence and stability region for vector solitons in two-component BEC with weak intercomponent repulsion ( $\sigma = -0.5$ ). One of the component either  $N_1$  or  $N_2$  vanishes at the edge of the existence domain restricted by black solid line. Between green and black line vector solitons are *completely stable*. Blue line is the boundary of collapse-free region: soliton solutions with chemical potential from the region restricted by blue and green lines are stable with respect to collapse, but they are unstable with respect to snake-type instability: mode with  $L = 1$  is unstable, while growth rates for  $L = 2$  mode are equal to zero. Finally red line separate solutions, which are unstable with respect  $L = 2$  as well as to  $L = 1$  modes: growth rates for both  $L = 1$  and  $L = 2$  azimuthal modes are positive.

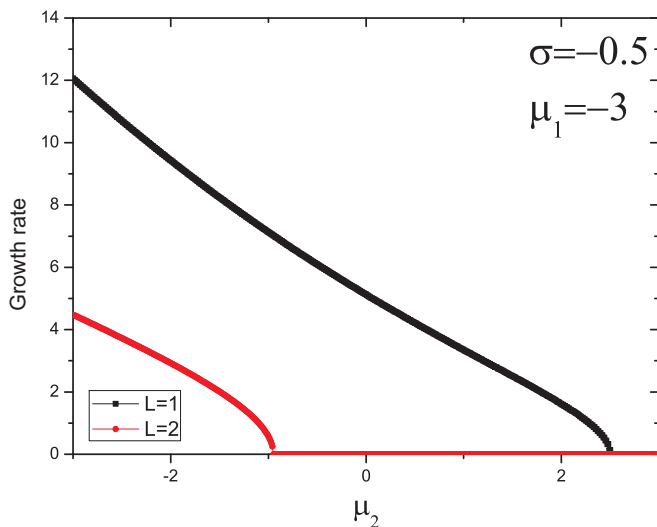


FIG. 6: (Color online) Maximum growth rates as the functions of  $\mu_2$  at fixed  $\mu_1$ . Note that all growth rates vanish above some threshold value of  $\mu_2$ .

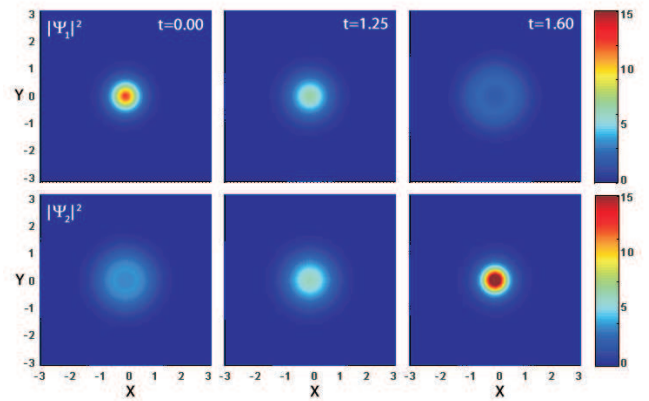


FIG. 7: Collapse. Here  $\sigma = -0.5$ ,  $\mu_1 = -0.5$ ,  $\mu_2 = 1$  (point 2 in Fig. 5).

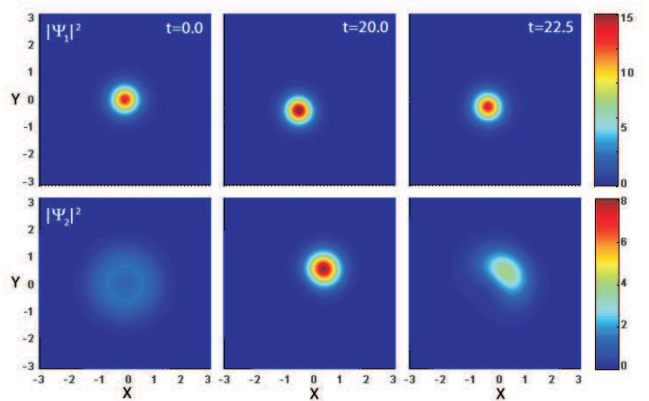


FIG. 8: Instability with respect to mode  $L=1$ . Here  $\sigma = -0.5$ ,  $\mu_1 = -1.5$ ,  $\mu_2 = 2$  (point 1 in Fig. 5).

sive inter-component interactions. Development of this instability leads to spatial separation of solitonic components (see Fig. 8) Nevertheless, using an appropriate perturbation with  $L = 2$  it is possible to observe a decay of shell component into two filaments (see Fig. 9) and further collapse of these filaments. To summarize our studies of the linear stability we present a green line which separate completely stable and unstable with respect to  $L = 1$  azimuthal mode solitons in Fig. 5. In this figure red lines present the edge of the instability region with respect to mode  $L = 2$ .

(iii) These results have been confirmed by direct numerical experiments on nonlinear dynamics of perturbed vector solitons. We present the region of stability, obtained by direct numerical simulations by square symbols in Fig. 5. Note an excellent agreement between predictions of linear stability analysis and direct numerical simulations.

The typical examples of unstable evolution are given in Figs. 7,8,9. We note that the simple mean field model gives a reasonable approximation for most reported here

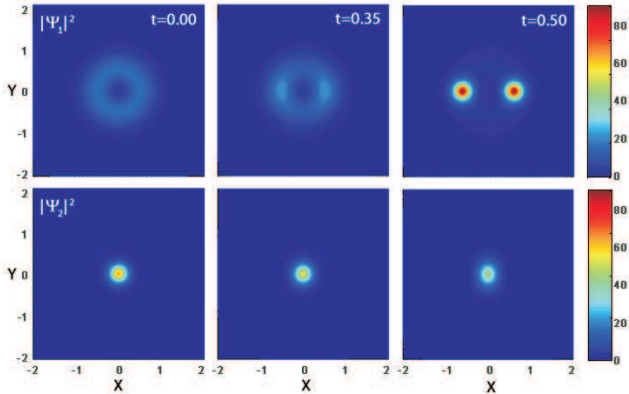


FIG. 9: Instability with respect to mode  $L=2$ . Evolution of the  $|\psi_j|^2$  for  $\sigma = -0.8$ ,  $\mu_1 = -5$ ,  $\mu_2 = -5$ .

evolutionary scenarios, however a mean-field approach fails when collapse develops so the atomic density catastrophically increases.

If only one component has more than  $N_{cr}$  particles (where  $N_{cr} = 11.68$  - number of particles in Townes' soliton) more powerful component is unstable with respect to collapse. The corresponding snapshots of  $|\psi_1|^2$  and  $|\psi_2|^2$  are given in Fig.7. In this case  $N_1 = 11.18$  and  $N_2 = 14.01$ . As is seen, internal component leaks out of the more powerful outer component. An attractive intra-component force shrinks a soliton with initial ring-type profile and finally it collapses.

An oscillations between quasicollapse and asymmetric state was observed (see Fig. 8), if both solitonic components have number of atoms below the critical value  $N_{cr}$  and the growth rate for  $L = 1$  mode is not equal to zero. If the number of particles in one component is more than  $N_{cr}$ , such oscillations continue few cycles only, and collapse (instead of quasicollapse) of the most powerful component takes place.

Growth of  $L = 2$  mode leads to decay of the shell solitonic component into two filaments. First two humps and two holes appear in the ring, and internal component rapidly leaks through these hollows in a ring-shape "potential well". Repulsive inter-component interaction between ring-shaped soliton and leaking internal soliton leads to increasing the hollows and finally ring breaks into two separated parts. We found that collapse of both filaments occurs, if number of particles in ring-shaped soli-

ton is greater than  $2N_{cr}$ . In case of  $N_{cr} < N < 2N_{cr}$  vector solitons execute oscillations for a long time. An example of such evolution is given in Fig.9. We have observed in our numerical simulations that, if inter-component interaction is not strong enough, collapse of the most powerful component occurs before instability with respect to mode  $L = 2$  appears.

The stability region shrinks dramatically when strength of repulsive interaction approaches  $\sigma = -1$ . Nevertheless, we have found that stable vector solitons exist even for strong repulsive inter-component interactions when  $\sigma < -1$ . The stability properties as well as detailed analysis of stationary solutions for this case will be published elsewhere.

## V. SUMMARY AND CONCLUSIONS

Fundamental 2D soliton-soliton pairs are investigated in two-component BEC with attractive intra-component interactions. General properties of vector solitons are studied analytically and numerically both for attractive and repulsive inter-component interactions.

Matter-wave bright vector solitons are found to be always stable for attractive inter-component interactions. The eventual destabilization can be caused by repulsive interactions between atoms of different components. Various unstable evolution scenarios including collapse and azimuthal symmetry-breaking instabilities are revealed for fundamental soliton-soliton pairs with repulsive inter-component interactions. The instabilities lead to separation of the condensate phases and further collapse of stronger over-critical component or periodical relative motion of the below-critical solitonic components backwards and forwards near the bottom of trapping potential. Using linear stability analysis of azimuthal perturbations and direct numerical simulations of evolution of perturbed steady states we predict stabilization of vector matter-wave solitons.

## VI. ACKNOWLEDGMENT

The work was supported by the grants WE1085/5-1 (DFG, Germany), A/11/05264 (DAAD, Germany), and F39.2 (SFFR, Ukraine). We thank V.M. Lashkin for useful discussions.

[1] F. Dalfovo, S. Giorgini, L.P. Pitaevskii, S. Stringari, *Reviews of Modern Physics*, 1999, pp.463 - 512.  
 [2] A.I. Yakimenko, V.M. Lashkin, O.O. Prikhodko *Phys. Rev. E*, **73**, 066605 (2006)  
 [3] A.I. Yakimenko, Yu.A. Zaliznyak, V.M. Lashkin *Phys. Rev. A*, **79**, 043629 (2009)  
 [4] A.I. Yakimenko, O.O. Prikhodko, and S.I. Vilchinsky

*Phys. Rev. E*, **82**, 016605 (2010)  
 [5] X.Liu, H.Pu, B.Xiong, W.M. Liu, J. Gong, *Phys. Rev. A*, **79**, 013423 (2009)  
 [6] J. N. Malmberg, A. H. Carlsson, D. Anderson, M. Lisak, E. A. Ostrovskaya, and Yu. S. Kivshar, *Opt. Lett.* **25**, 643 (2000).  
 [7] V.I. Petviashvili and V.V. Yan'kov, *Rev. Plasma Phys.*

- Vol. 14, Ed. B.B. Kadomtsev, (Consultants Bureau, New York, 1989), p 1.
- [8] H. Pu and N.P. Bigelow, *Phys. Rev. Lett.* **80**, 1130 (1998).
- [9] T.-L. Ho and V.B. Shenoy, *Phys. Rev. Lett.* **77**, 3276 (1996).
- [10] B.D. Esry, C.H. Greene, J.P. Burke, Jr., and J.L. Bohn, *Phys. Rev. Lett.* **78**, 3594 (1997).
- [11] B. P. Anderson, P. C. Haljan, C. A. Regal, D. L. Feder, L. A. Collins, C. W. Clark, and E. A. Cornell, *Phys. Rev. Lett.* **86**, 2926 (2001); Th. Busch and J. R. Anglin, *ibid.* **87**, 010401 (2001).
- [12] P. Öhberg and L. Santos, *Phys. Rev. Lett.* **86**, 2918 (2001).
- [13] P.G. Kevrekidis, H.E. Nistazakis, D.J. Frantzeskakis, B.A. Malomed, and R. Carretero-González, *Eur. Phys. J. D* **28**, 181 (2004).
- [14] S. Coen, and M. Haelterman, *Phys. Rev. Lett.* **87**, 140401 (2001).
- [15] K. Kasamatsu, and M. Tsubota, *Phys. Rev. Lett.* **93**, 100402 (2004).
- [16] P.G. Kevrekidis, H. Susanto, R. Carretero-González, B.A. Malomed, and D.J. Frantzeskakis, *Phys. Rev. E* **72**, 066604 (2005).
- [17] V. M. Pérez-García and J. B. Beitia, *Phys. Rev. A* **72**, 033620 (2005).
- [18] D. V. Skryabin, *Phys. Rev. A* **63**, 013602 (2000).
- [19] J. J. García-Ripoll and V. M. Pérez-García, *Phys. Rev. Lett.* **84**, 4264 (2000).
- [20] V. M. Pérez-García and J. J. García-Ripoll, *Phys. Rev. A* **62**, 033601 (2000).
- [21] L. Li, B. A. Malomed, D. Mihalache, and W. M. Liu, *Phys. Rev. E* **73**, 066610 (2006).
- [22] H. Saito and M. Ueda, *Phys. Rev. Lett.* **89**, 190402 (2002).
- [23] H. Saito and M. Ueda, *Phys. Rev. A* **69**, 013604, (2004)